metals

MDPI

Review

Solidification Processing of Metallic Materials in Static Magnetic Field: A Review

Yuan Hou [1], Zhanyong Gao [1] and Chuanjun Li [2,*]

[1] Analytical and Testing Center, Inner Mongolia University of Science and Technology, Baotou 014010, China
[2] School of Iron and Steel, Soochow University, Suzhou 215137, China
* Correspondence: cjli21@suda.edu.cn

Abstract: The application of a static magnetic field (SMF) to solidification processing has emerged as an advanced strategy for efficiently regulating the macro/micro structures and the mechanical performance of metallic materials. The SMF effects have been proved to be positive in various processes of metal solidification. Firstly, this review briefly introduces two basic magnetic effects, i.e., magnetohydrodynamic effects and magnetization effects, which play crucial roles in regulating metal solidification. Further, the state of the art of solidification processing in the SMF, including undercooling and nucleation, interface energy, grain coarsening and refinement, segregation and porosity, are comprehensively summarized. Finally, the perspective future of taking advantage of the SMF for regulating metal solidification is presented.

Keywords: static magnetic field; magnetohydrodynamic effect; magnetization effect; undercooling; interfacial tension; dendrite coarsening; grain refinement; segregation; porosity; crystal orientation

check for updates

Citation: Hou, Y.; Gao, Z.; Li, C. Solidification Processing of Metallic Materials in Static Magnetic Field: A Review. *Metals* **2022**, *12*, 1778. https://doi.org/10.3390/met12111778

Academic Editors: Tadeusz Kulik and Evgeny A. Kolubaev

Received: 31 August 2022
Accepted: 17 October 2022
Published: 22 October 2022

1. Introduction

It is an extremely important topic to regulate the solidification processing of metallic materials, as it determines the micro/macro structures and, thus, the mechanical properties of the as-cast products [1,2]. Over the past century, a lot of effort has been dedicated to theoretical and experimental studies in the field of solidification and many milestone techniques and methods have been developed to obtain the required physico-chemical/mechanical properties of metallic materials [3,4]. As the solidification theories and processing methods are well-developed, the conventional routines with respect to regulating the solidification parameters, such as the cooling rate, undercooling and the temperature gradient, have entered the bottleneck stage [5]. From the point of view of the development of science and technology, it is never an outdated theme to explore new techniques and methods of solidification processing. Additionally, the developed and flourished world economy provides strong demand for high-quality and high-performance as-cast products, which also motivates the renovation of solidification processing methods.

In past decades, the emergence of effective strategies using external fields, such as magnetic field, electric field and ultrasonic field, has become a potential trend in the field of metal solidification processes, which can effectively regulate nucleation and growth and further modify solidification structures [6,7]. Owing to contactless interaction and various magnetic effects, the application of the magnetic field to solidification processing has attracted intensive attention [8–13]. The magnetic field is implemented in two types, i.e., the time-varying and static magnetic fields. In this review, we emphasize the state of the art of solidification processing in the static magnetic field (SMF). The numerous studies confirm that applying the SMF to metal solidification processes is a promising and novel strategy to modify nucleation [14], undercooling [15], interface free energy [16], grain coarsening [17] and refinement [18], segregation [19], and porosity [20]. Although the magnetic field has exerted significant effects on metal solidification processes, its applicability needs further development and the related physical mechanisms deserve further elucidation.

Although the effects of the SMF on solidification processing were reviewed with respect to orientation, melt flow, solidification structure, etc. [6], progress has been made in recent years and, thus, an updated review is warranted. This review firstly briefly introduce two magnetic effects, i.e., magnetohydrodynamic and magnetization effects. Further, recent reports regarding the SMF-regulated metal solidification processes are summarized, including undercooling, interface free energy, grain coarsening and refinement, segregation and porosity. In addition, in-situ and 3D imaging strategies have been developed to accelerate scientific discovery of the SMF-regulated solidification processing. Finally, the perspective future on the potential and challenge of SMF-regulated metal solidification processes is presented.

2. Principles of SMF-Regulated Metal Solidification

In principle, the SMF exerts an effect on metal solidification through two mechanisms: (1) a magnetohydrodynamic (MHD) effect resulting from the Lorentz force; and (2) magnetization effect originating from the magnetic force.

2.1. Magnetohydrodynamic Effect

It is well-known that an SMF changes the melt flow, e.g., electromagnetic braking [21] and thermoelectromagnetic convection (TEMC) [6,22,23]. The former is used to suppress fluid flow and widely applied to industrial production such as continuous casting. The latter induces interdendritic forced convection and further modifies solidification structures. In principle, the above-mentioned magnetohydrodynamic effects originate from the interaction between the SMF and the electric current.

Ohm's law relates the electric current density to the generalized electric field (E) by

$$j = \sigma E + \sigma u \times B - \sigma S \nabla T \tag{1}$$

where σ is the electric conductivity, u is the velocity, ∇T is the temperature gradient and S is the thermo-electric power of the medium. The term σE is the current directly generated by the applied electric field. The term $\sigma u \times B$ is known as the induced current, owing to fluid flow. The term $\sigma S \nabla T$ is the internal electric current near the interface owing to the thermoelectric effect.

In the SMF, the Lorentz force F_{EM} is expressed as

$$F_{EM} = j \times B \tag{2}$$

Assuming that the fluid is incompressible, the fluid flow is governed by Navier–Stokes equation.

$$\begin{gathered} \rho \frac{\partial u}{\partial t} + \rho (u \cdot \nabla u) = -\nabla p + j \times B + \rho \nu \nabla^2 u \\ = -\nabla p + \sigma E \times B + \sigma (u \times B) \times B - \sigma S \nabla T \times B + \rho \nu \nabla^2 u \end{gathered} \tag{3}$$

This combines with the mass conservation equation:

$$\nabla \cdot u = 0 \tag{4}$$

where ρ is the density of the fluid, p is the pressure and ν is the kinematic viscosity of the fluid.

From Equation (3), one can obtain that the term $\sigma(u \times B) \times B$ is the braking force, whereas $\sigma S \nabla T \times B$ is a driving force for the fluid flow. During dendrite growth in the SMF, the contributions of two effects to the melt flow vary when increasing the SMF [6].

Additionally, the thermoelectromagnetic force (TEMF), which stems from the internal electric current acting on the dendrite (F'_{TE}), can be written as

$$F'_{TE} = \frac{\sigma_L \sigma_S f_L}{\sigma_L f_L + \sigma_S f_S} (S_S - S_L) \nabla T B \tag{5}$$

where the subscripts S and L denote the liquid and solid, respectively. The TEMF leads to the formation of numerous dislocations in the dendrites and even to fragmenting the dendrite, which have been observed in previous studies [6].

In summary, the thermoelectromagnetic effects during dendrite solidification are schematically described in Figure 1 [24].

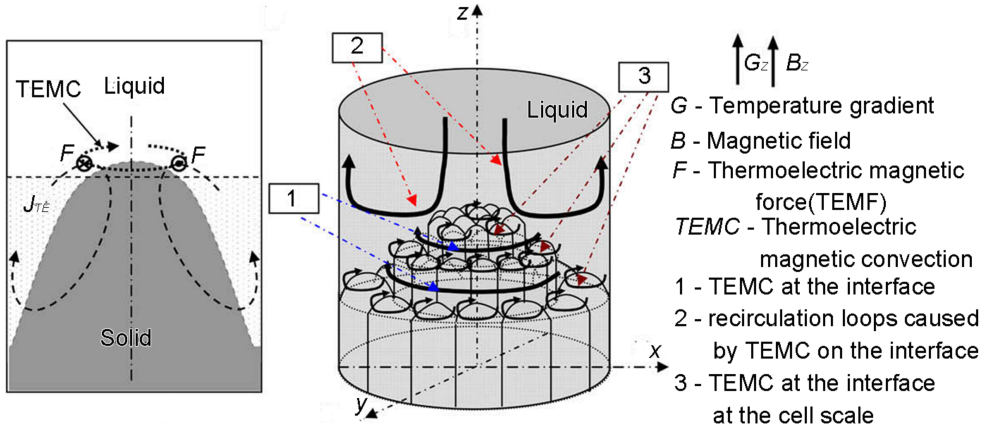

Figure 1. A schematic illustration of the thermoelectromagnetic effects [24].

2.2. Magnetization Effect

Since every substance has its own magnetism, scientists hope to use magnetism to control metal solidification processes. The magnetism can be characterized using magnetic susceptibility, which is defined using the following equation.

$$M = \chi H \tag{6}$$

where χ is the volume magnetic susceptibility, M is the magnetic magnetization, and H is the magnetic field strength. The magnetic susceptibility closely relates to some magnetic effects, such as the magnetic force and orientation.

When the metal is placed in the magnetic field gradient, it is subjected to the magnetic force (F_m), which is written as:

$$F_m = \mu_0 (M \cdot \nabla) H = \frac{\chi}{\mu_0} (B \cdot \nabla) B \tag{7}$$

The magnetic force can be used to separate minerals, to levitate the substances, and to control flow.

Additionally, the magnetization energy of the material is induced by the SMF and it is defined as

$$E_m = -\int_0^H \mu_0 M dH \tag{8}$$

The magnetization energy may modify the phase boundary, kinetics of phase transformation, orientation and microstructures [25]. The orientation is schematically described in Figure 2.

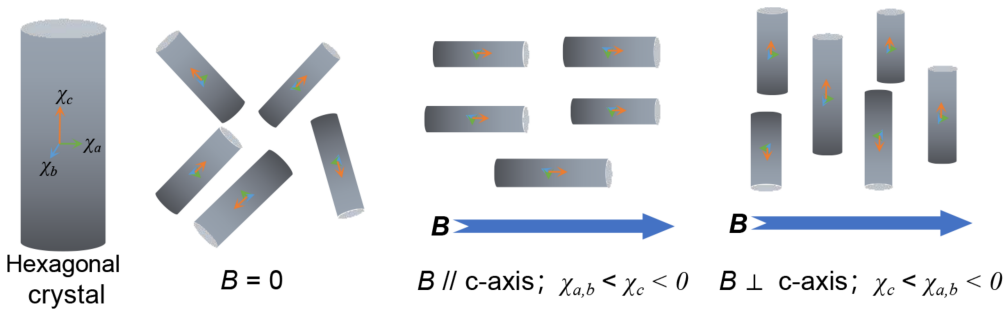

Figure 2. A schematic illustration of magnetic alignment of hexagonal crystals.

3. SMF-Regulated Metal Solidification

As mentioned above, there have been excellent reviews regarding solidification processing of metallic materials, as referred to in the literature [5–8,10,12,13,26]. The objective of this section is to summarize the research findings in recent years.

3.1. SMF Effects

3.1.1. SMF-Induced Undercooling

The degree of undercooling is an important parameter affecting metal solidification. A large undercooling can refine grains, reduce segregation and realize non-equilibrium effects [14,15]. It was found that the SMF changed the undercooling of different metal melts and some possible explanations were proposed, such as the delayed formation of the nucleation-catalyzed oxides [27] and the increase in solid/liquid interfacial tension due to the magnetic dipolar interaction [28]. Nevertheless, these explanations are not convincing.

Typically, a recent work regarding the change in the undercooling of Sn, Al, Zn and three Al-Cu alloy melts in different SMFs was performed by Rui Guo and his co-workers [29–31] (Figure 3). They proposed that the change in undercooling is related to the increase in the liquid/solid interfacial free energy and to the reduction in migration rates of atoms in the liquid phase in the SMFs. This mechanism is schematically illustrated in Figure 3. When the movement direction of liquid atoms is not parallel to the SMF, these atoms will spirally move and the probability of a collision with other atoms will increase under the influence of Lorenz force. This leads to an increase in the transferring time of the atom to nucleus, which, in turn, enhances the undercooling.

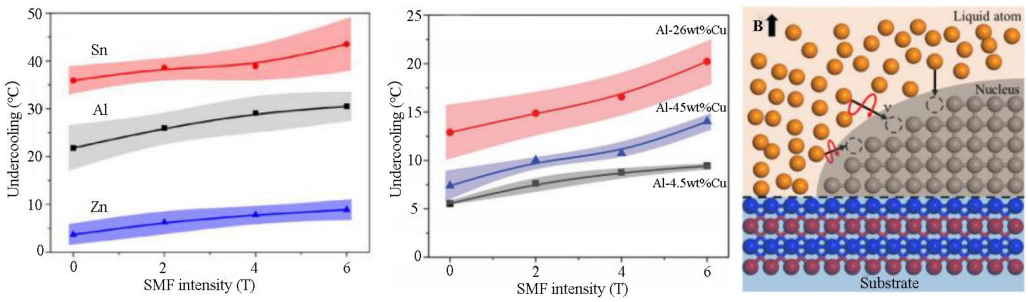

Figure 3. Undercoolings of the primary phases of different metals and schematic illustration of spiral motion of a liquid atom attaching to a nucleus in SMFs [29,30].

Wang et al. systematically investigated the effect of the SMF on the degree of undercooling [32,33]. It was found that the undercooling for homogeneous nucleation is irrelevant to the SMF intensity, but influenced undercooling for heterogeneous nucleation, as shown in Figure 4. It was thought that the phenomena can be interpreted using magnetohydrodynamic effects. Interestingly, they found that the highest temperature after recalescence is altered by the SMF and the gradient SMF depressed the mean undercooling.

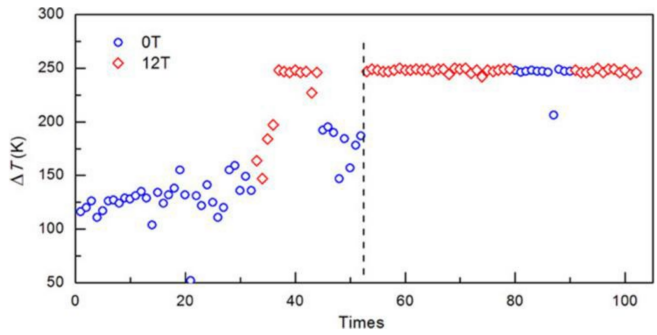

Figure 4. Dependence of cyclic heating times on the undercooling of Cu under 0 and 12 T SMF [32].

3.1.2. Additional Interfacial Tension Induced by SMF

The interface tension influences the nucleation, growth and morphology [1]. In light of the importance of interface phenomena, some attempts have been made to explore the change in the interfacial tension of inorganic liquids in an SMF [34,35]. Recently, investigation into the interfacial properties of metallic systems in an SMF have been presented [36–41].

Li et al. investigated the change in the wettability of a solid by a liquid metal in the SMF [16]. They applied a sessile drop technique to systematically observe the effect of an SMF on the wettability of copper and silica substrates by a Ga-In-Sn liquid alloy, respectively (Figure 5). It was found that the contact angles on both substrates increased with increasing the SMF intensity. The reduced wettability can be attributed to the change in liquid surface tension under the action of an SMF. They further developed an equation to predict the variation in the contact angle with the SMF intensity, as follows

$$\frac{1+\cos\theta}{1+\cos\theta_m} = 1 + \frac{1}{3}BL\sqrt{\frac{\sigma}{\eta}} \tag{9}$$

where θ and θ_m are the contact angles with and without an SMF; and B, L, σ and η are the SMF intensity, characteristic length, electric conductivity and viscosity, respectively. The above equation can reasonably predict the wettability as a function of the SMF intensity, as shown in Figure 5.

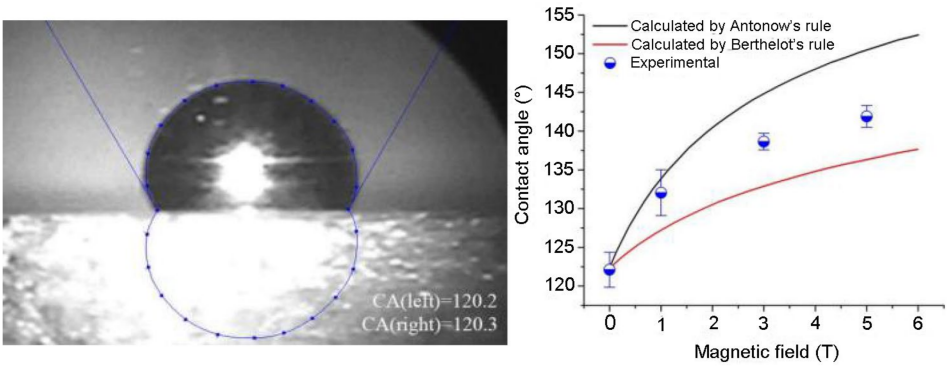

Figure 5. Determination of the left and right contact angles of a drop on the copper substrate and comparison between experimental and calculated contact angles in SMFs [16].

More recently, Huang et al. performed experiments of measurement solid/liquid interfacial free energy of Al-Cu alloy system under SMF [42]. They improved the grain boundary groove method to measure the interfacial free energy. It was found that the interfacial free energy between the solid α-Al and liquid Al-Cu system increased by 31.5%, while this value of the solid $CuAl_2$-liquid Al-Cu system was found to decrease by 46.17%. The microstructure showed that the $CuAl_2$ phase nucleated on the surface of α-Al phase and, thus, the high Cu concentration in the liquid phase was formed. The entire liquid

Cu-rich phase has diamagnetism due to the magnetic susceptibilities of the atoms in the liquid phase (Figure 6). It follows that the SMF promotes the formation of magnetic dipoles on the solid–liquid interface and, thus, resulted in the change in the surface tension.

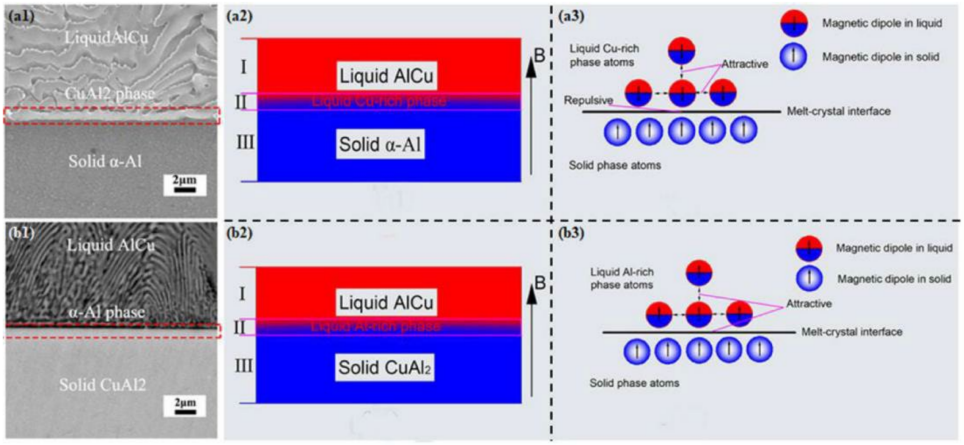

Figure 6. Schematic of magnetic dipole–dipole interactions in the liquid metal bulk and at the solid α-Al (**a1**–**a3**) and $CuAl_2$ (**b1**–**b3**) in equilibrium with the eutectic Al-Cu liquid interface.[42].

3.1.3. Dendrite Coarsening in SMF

The dendritic growth kinetics of crystals is one of the important issues in various processes of metal solidification. Gao et al. measured the dendritic growth velocities of pure nickel in the SMF [43,44]. Dendrite coarsening, as an aspect of dendritic growth, affects the final secondary dendritic arm spacing (SDAS) and, thus, plays a crucial role in microsegregation [45–52]. Some investigations imply that the SMF possibly modifies the coarsening of dendrites [53–56]. Nevertheless, there has been no work on coarsening kinetic under the SMF.

He et al. investigated dendrite coarsening in the Al 4.5 wt% Cu alloy in the SMF by the quenching technique [17]. The experimental results showed that the SDAS increased in the SMF (Figure 7), which is attributed to the TEM convection as well as the change in solid/liquid interfacial tension. The coarsening of SDAS in the SMF led to a long diffusion path across the dendrite arm and enlarged the microsegregation level.

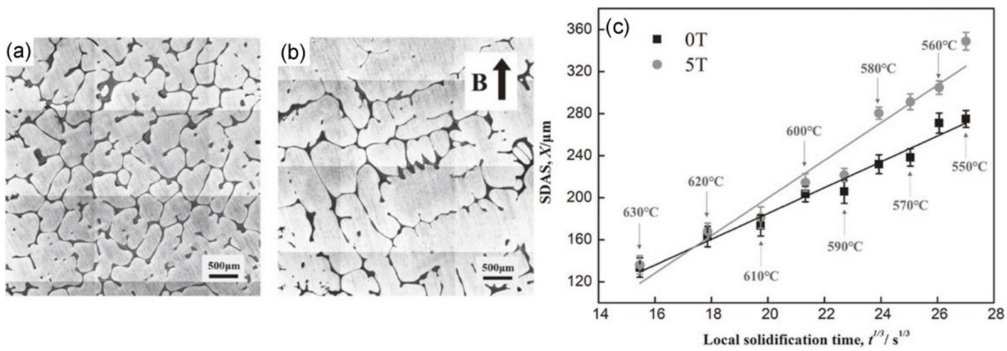

Figure 7. Longitudinal microstructures (**a**,**b**) and SDAS against the cubic root of local solidification time (**c**) of the Al 4.5 wt% Cu alloy quenched by the rate of 0.3 °C/min at 560 °C without and with 5 T SMF [17].

3.1.4. SMF-Induced Grain Refinement

The grain refinement is beneficial for improving the mechanical performance [57–60]. Conventionally, the adding of the grain refiner or increasing the cooling rate are the preferential methods for grain refinement [61–63]. Nevertheless, those methods have some limitations, e.g., the grain refiner either increases the content of impurities or the effective

grain refiner lacks a given alloy. The cooling rate is hardly changed in a large ingot. It was found that the SMF provides a potential method for grain refinement. The grain refinement has been observed in the solidified Al-base alloys, Pb–Sn alloys and Ni base superalloys under an SMF [18,64–66]. Recently, our group took advantage of the TEM effect to refine grains in directionally solidified GCr18Mo steel (Figure 8) [67]. We found that the grain refinement was enhanced with the increase in the SMF intensity and in temperature gradient but the refinement was weakened with a decrease in the growth speed. The enhancement of the grain refinement in the SMF can be rationalized by the TEM convection in the melt and the TEM force acting on the dendrite during directional solidification.

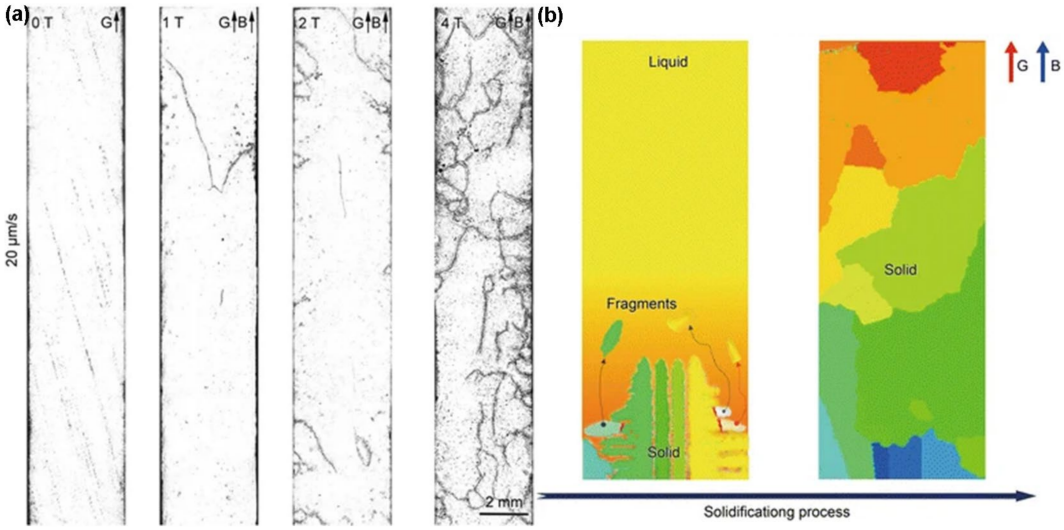

Figure 8. Longitudinal solidification structures (**a**) of GCr18Mo steel at different SMF intensities and growth speeds under temperature gradient of 104 K/cm, corresponding to the schematic illustration of grain refinement (**b**) [67].

Meanwhile, the SMF can reduce the microsegregation level in the directionally solidifying GCr18Mo steel. Figure 9 presents that the fluctuation range of the Cr content at the position of 20 mm from the solid/liquid interface decreases as the SMF intensity increases.

Further, we obtained a process window for the columnar to equiaxed transition of GCr18Mo steel in SMFs (Figure 10) [68]. Applying 5 T SMF can form equiaxed grains below the cooling rate of 0.312 K/s under the temperature gradient of 104 K/cm, which may potentially be used to control the columnar to the equiaxed transition of the steel casting ($10^{-1}-10^{0}$ K/s).

3.1.5. SMF-Controlled Segregation

The reduction in the microsegregation level during solidification can shorten the subsequent heat treatment process and also improve the mechanical performance [47,69,70]. Previous experimental studies have shown that the SMF was capable of modifying the extent of microsegregation during alloy solidification [19,71–74]. However, these studies were mostly limited to qualitative analysis with respect to the effect of the SMF on segregation. He et al. experimentally investigated the microsegregation formation of two Al-Cu alloys directionally solidified in the SMF and theoretically explored the contributions of various processing factors such as undercooling, back diffusion, dendrite coarsening and melt flow to microsegregation using the modified microsegregation model (Figure 11) [75]. It was found that the microsegregation level was alleviated for cellular and dendritic growth while the amount of microsegregation increased for planar growth under the SMF. Considering contributions of the change in various factors in an SMF, the change in the microsegretation level was in agreement with the experiment result.

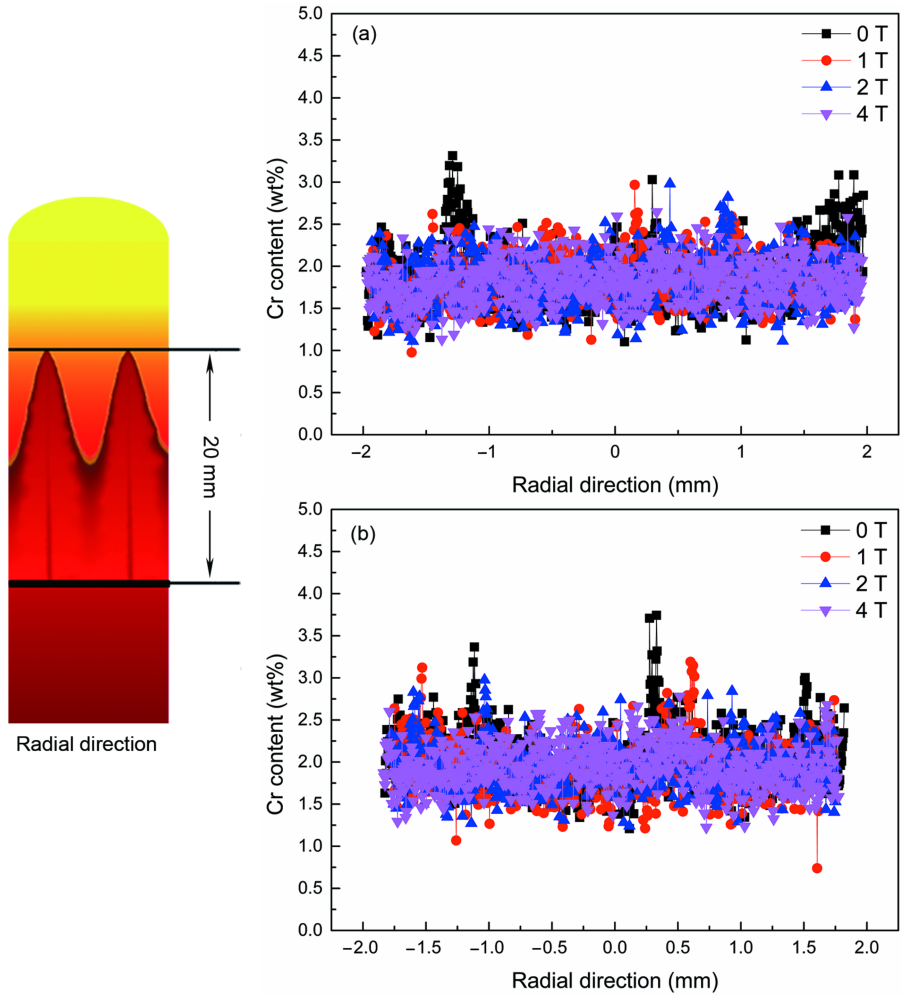

Figure 9. Cr contents for radial profiles in solid at 20 mm from the solid/liquid interface (indicated by the graph on the left) fabricated under temperature gradient of 104 K/cm with growth speeds of 10 μm/s (**a**) and 20 μm/s (**b**) [67].

3.1.6. SMF-Controlled Porosity

The shrinkage porosity due to the sample shrinkage or volume variation at the final stage of solidification plays a negative role in the hot rolling and final performance of the metallic materials [2,57,76]. Adopting effective strategies to eliminate the shrinkage porosity is one of the most attractive research subjects for metallurgists [77–80]. By imposing a 29 T SMF, Zheng et al. found the morphologies of shrinkages are changed to approximately regular spheres and the average volume of shrinkages become larger, resulting from the suppression of melt convection (Figure 12) [20].

Nevertheless, the TEM convection occurs ahead of solid/liquid interface and accelerates the motion of fluid in the mushy zone. The present authors systematically investigated the effect of TEM convection on the shrinkage porosity at the final stage of the solidification of GCr18Mo steel in the SMF (Figure 13) [81]. It was found that the amount of porosity first decreases and then increases with increasing the SMF intensity. The decrease in porosity is attributed to an adequate development of the TEM convection, which leads to sufficient feeding. This study sheds light on an alternative technique for eliminating the shrinkage porosity at the final stage of alloy solidification in industrial applications.

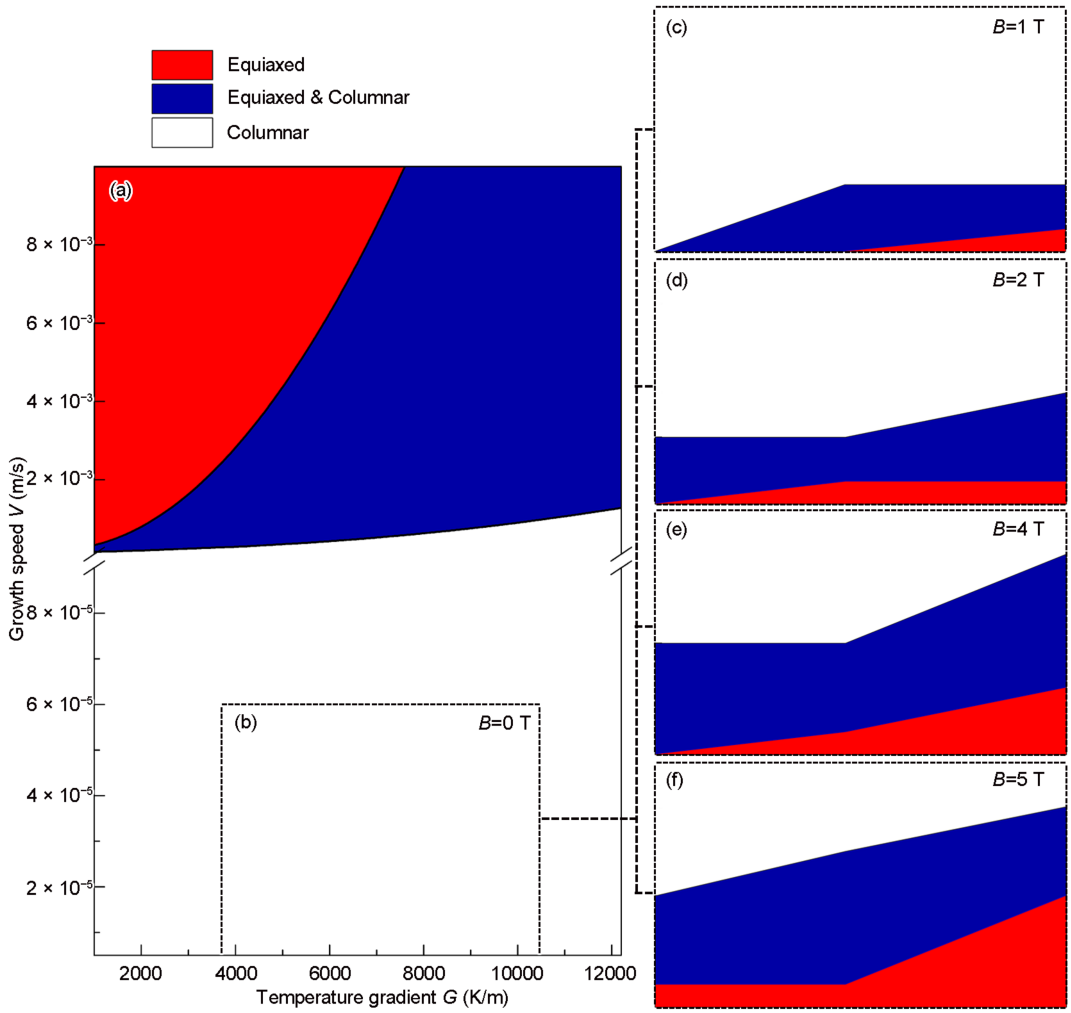

Figure 10. Microstructure selection map for GCr18Mo steel calculated by the Hunt's model (**a**) and experimentally obtained from the different SMF intensities (**b**–**f**), when the imposed temperature gradient or growth speed are varied.[68].

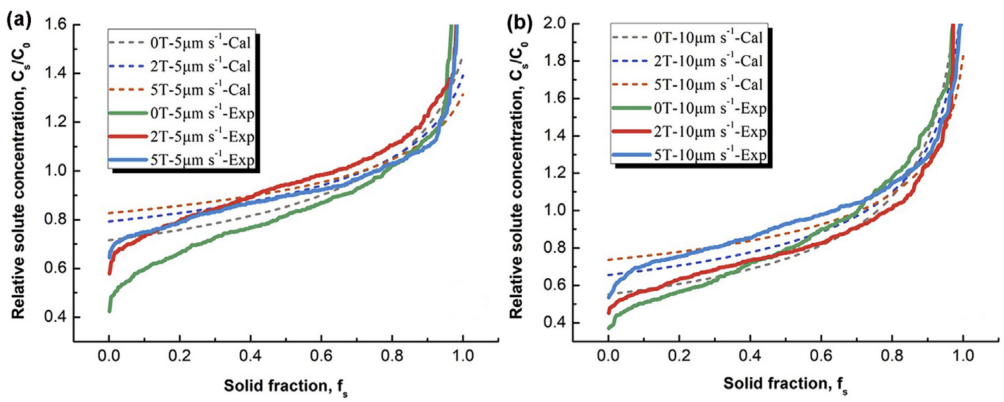

Figure 11. Comparisons of the calculated and experimental results of concentration versus solid fraction curves for Al-Cu alloys during directional solidification [75]. (**a**) Al-0.85wt.%Cu alloy, (**b**) Al-4.5wt.%Cu alloy.

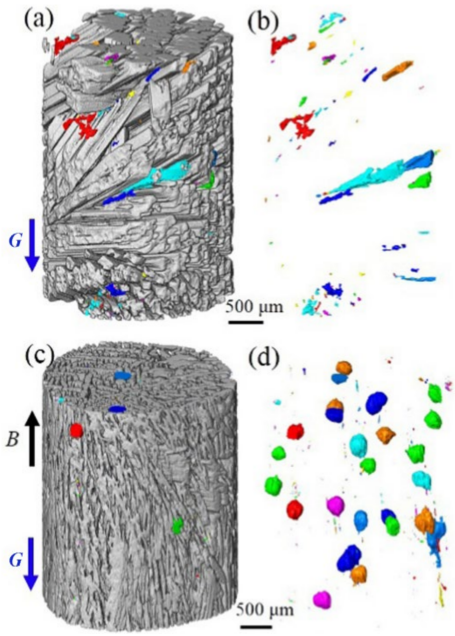

Figure 12. 3D distribution and morphologies of shrinkages: (**a**,**b**) 0 T; (**c**,**d**) 29 T [20]. Colorful elements mean the shrinkage is independent each other in the adjacent region.

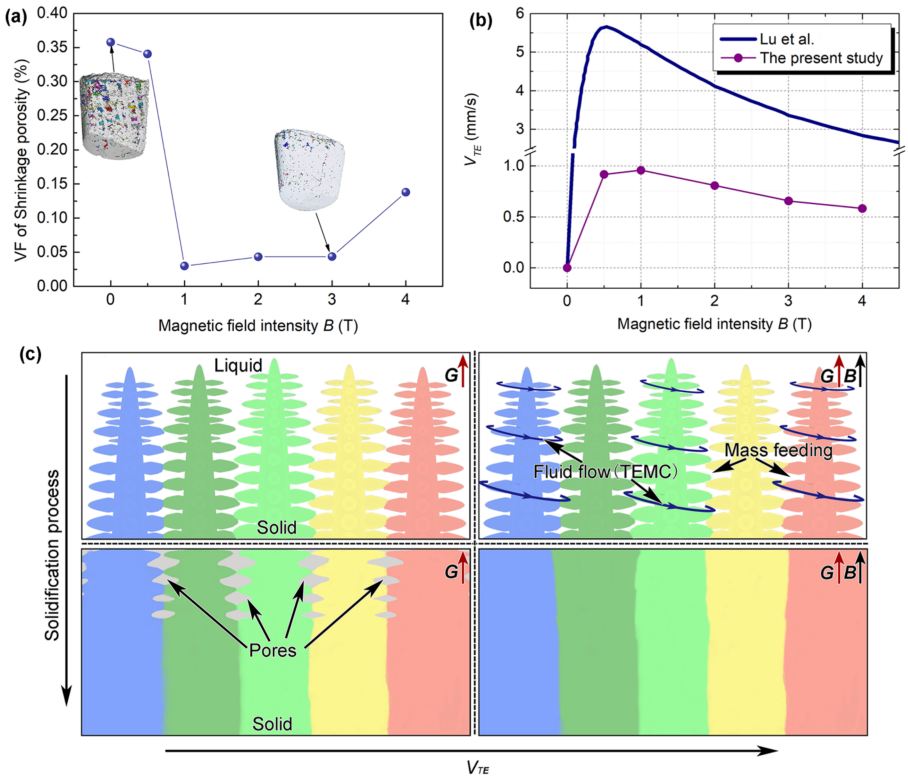

Figure 13. The volume fraction (VF) of the shrinkage porosity (**a**) and the maximum of the computed TEMC (**b**) near the final stage of solidification of a GCr18Mo steel under various SMFs, corresponding to the schematic illustration of the shrinkage porosity evolution (**c**) [81].

3.1.7. Crystal Orientation in SMF

Magnetic orientation is one of the important magnetic effects [82,83]. Various alloys, including Zn-Bi alloy [84], Bi-Mn alloy [85], Al-Fe alloy [86], Fe-Tb alloy [87], etc., have been employed to orient in the SMF. Recently, the SMF was used to fabricate the oriented silicon

steel, which has excellent magnetic properties such as high magnetic permeability and low core loss. Nevertheless, it is hard to obtain [1 0 0] crystal orientation by conventional methods [88,89]. Liu et al. investigated the influence of a high SMF on the crystal orientation and magnetic properties of the Fe-4.5 wt% Si alloy (Figure 14) [90]. It was found that the crystal orientation of the Fe-4.5 wt% Si alloy turns to the easy magnetization axis [1 0 0] with the increase in magnetic field intensity due to the magnetization force on the Fe-4.5 wt% Si alloy. In addition, the oriented Fe–6.5 wt.% Si–0.05 wt.%B and Fe-1.0 wt.% Si alloy were also obtained through controlling the crystallization process and adjusting the magnetic field intensity [91,92].

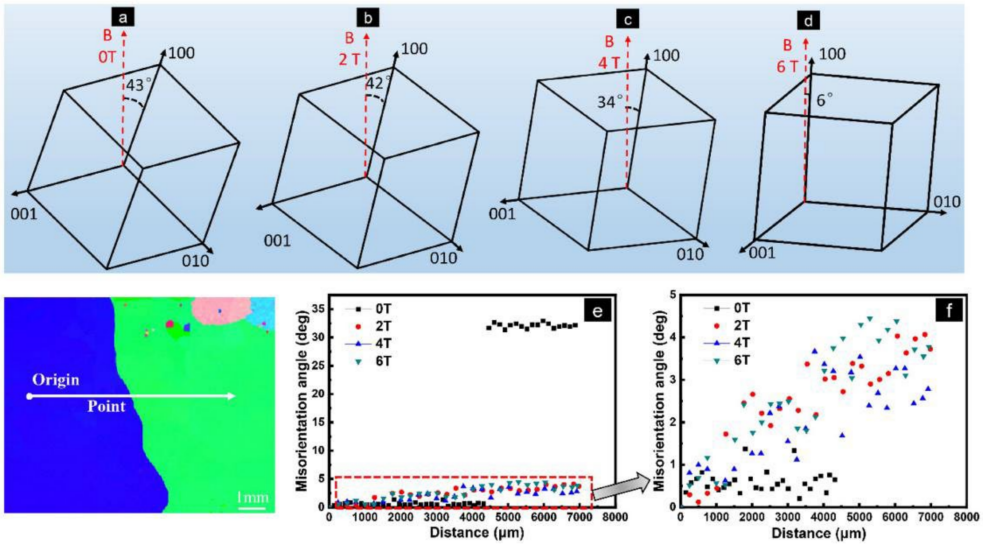

Figure 14. Schematic diagram (**a**–**d**) and misorientation angle from point-to-origin along the white line (**e**,**f**) of the crystal rotation orientation under different SMFs [90].

3.2. Possible Application of SMF to Rapid Solidification

Additive manufacturing has been gaining increasing attention in recent years [93–96]. Additive manufacturing has significant features, such as a high temperature gradient and rapid solidification at the micro-sized molten pool [97–99]. In this case, appreciable TEM convection most likely appears. Following the idea, Zhao et al. applied an SMF to the laser additive manufacturing in order to achieve the refined grain structure and to enhance mechanical properties without post-treatment and composition changes (Figure 15) [100]. It was found that the SMF of 0.55 T changed the microstructure with twisted prior-β grains (strong <001> orientation to weak <110> orientation) and discontinuous α grain boundaries. The sample without the SMF displayed coarse columnar prior-β grains, whereas the sample with SMF displays refined columnar prior-β grains.

Apart from additive manufacturing, a number of researchers have reported that the SMF exerted a significant effect on rapid solidification, including pool morphology and microstructure evolution [101–104]. However, the application of the SMF to advanced manufacturing is still a new field and there are quite a few fundamental scientific questions to be addressed.

3.3. Application of Synchrotron X-ray Imaging to Solidification with SMF

The in-situ synchrotron X-ray imaging technology is a powerful tool for revealing the physical mechanisms of various solidification phenomena [105–107]. In consideration of amazing magnetic effects to be clarified, it is of significance to applying the advanced synchrotron X-ray imaging technology to observe dendrite growth in the SMF [108–112].

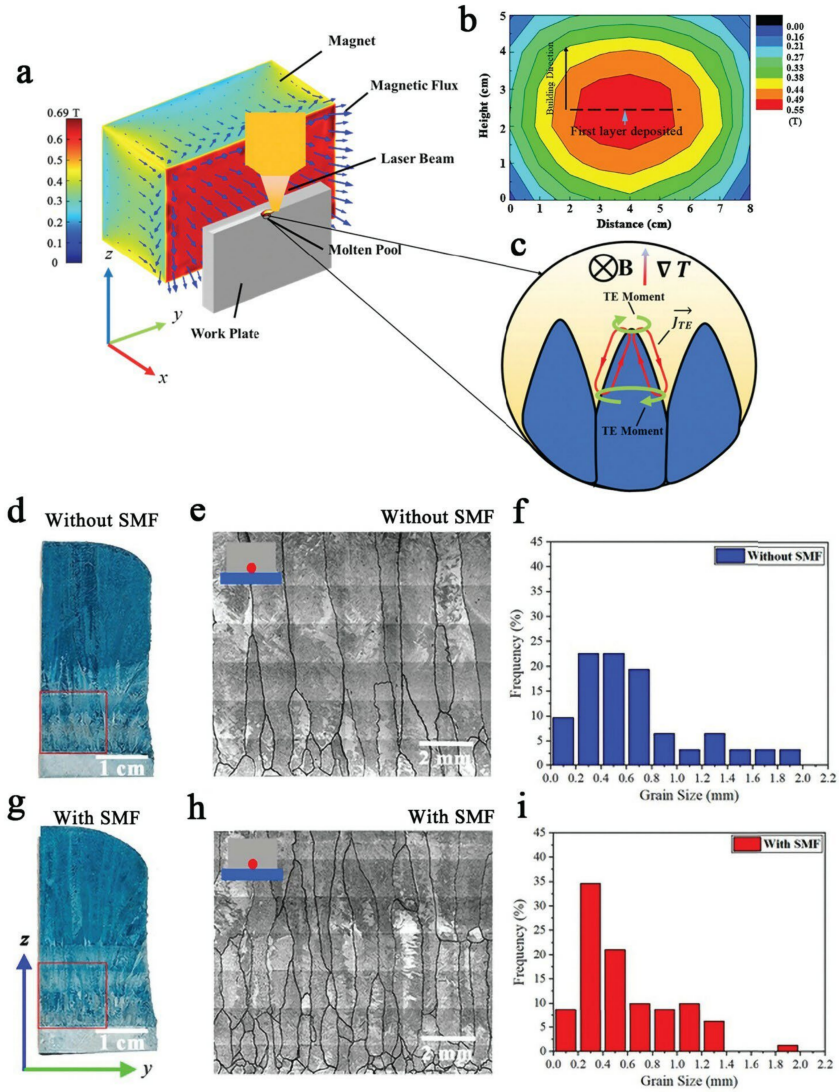

Figure 15. Schematic diagram of the solidification process of laser-direct energy deposition under a 0.55 T SMF (**a**), corresponding to the thermoelectric current and thermoelectric magnetic force in the solidification front (**c**), distribution of magnetic field intensity (**b**), optical microscopy images (**d**,**g**), β grains microscopy images (**e**,**h**) and histograms of β grain size (**f**,**i**) [100].

Applying in-situ synchrotron X-ray imaging, Wang et al. found the motion of detached fragments of dendrite in Al-4 wt.% Cu in a weak SMF [113]. Abou-Khalil et al. took a step further to gain the trajectory and velocities of the equiaxed grains during the solidification of Al-10 wt% Cu alloys, which were in good agreement with the numerical prediction (Figure 16) [114]. Cai et al. employed high-speed synchrotron X-ray tomography and computational simulation to reveal the mechanisms disrupting the columnar dendritic growth and demonstrated that the effect of the MHD can be changed by adjusting the alloy composition, which provides novel methods for optimizing the application of MHD during alloy solidification [115].

A 2D metallography or SEM observation is insufficient to elucidate the effect of the SMF on 3D dendritic morphology and the solid/liquid interface shape, especially the TEM convection ahead of the solid/liquid interface [116]. In-situ synchrotron X-ray imaging technology can give insight into the 3D dendrite morphology. Shuai et al. observed the 3D solid/liquid interface morphology and dendrite growth direction of Al-10 wt.% Zn alloy directionally solidified in the SMF of 5 T using X-ray micro-computed tomography (Figure 17a,b) [117]. In addition, the formation and growth dynamics of intermetallic

compounds in a Al-10 wt.% Si-1 wt.% Fe alloy during solidification in the SMF were exhibited using synchrotron X-ray tomography (Figure 17c). This work provides the possibility of regulating the precipitation behavior of Fe-rich intermetallic compounds in Al alloys [118].

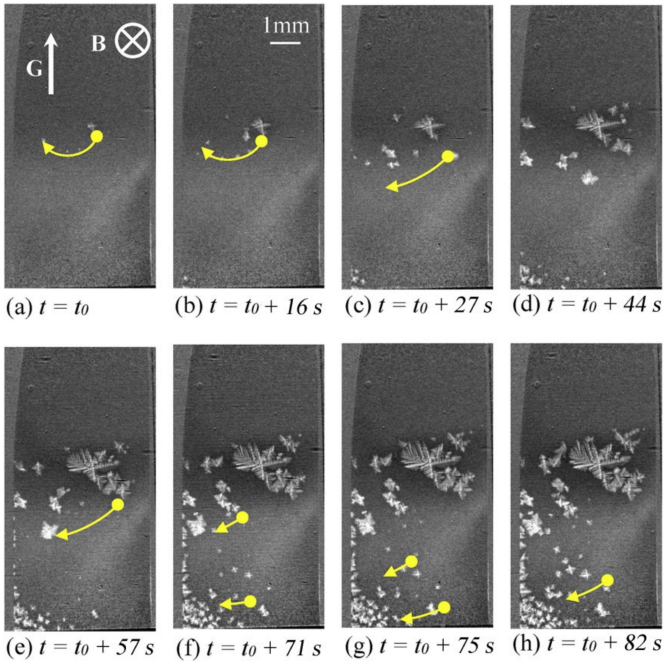

Figure 16. Sequence of radiographs of the equiaxed solidification experiment of Al-10 wt% Cu under 0.08T SMF at a cooling rate of 2 K/min and a temperature gradient of 20 K/cm [114].

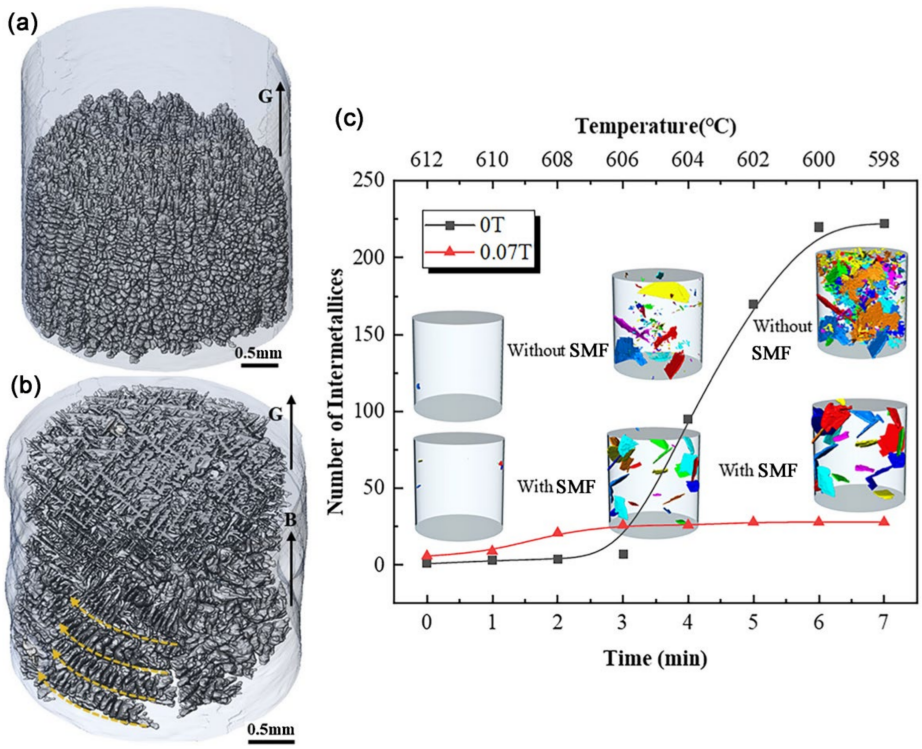

Figure 17. A number of 3D renderings of mushy zone areas or interface shapes of directionally solidified Al-10 wt.% Zn alloy (**a**,**b**) without and with a 5 T SMF; the precipitation number of iron intermetallic compounds varies with temperature and time (**c**) [117,118].

4. Conclusions and Perspective

SMF-regulated metal solidification is a novel strategy to improve the solidification structures and mechanical properties of as-cast products. The SMF can generate the electromagnetic force and the magnetic force to modify the solidification processes, such as undercooling and nucleation, interface tension, grain coarsening and refinement, segregation, and porosity. Although much effort has been made to investigate solidification processing in the SMF, there are still a lot of fundamental and practical aspects to be addressed in the future.

(1) Development of low-cost and large-bore strong magnets

Over the past two decades, research has been very active in the field of materials processing in the SMF and many novel findings have been obtained. However, most studies are still performed in laboratories and almost no findings on the SMF have been applied to industrial products (beside nuclear magnetic resonance and single crystal silicon growth). One of the important limits is the lack of low-cost and large-bore strong magnets. It is necessary to develop low-cost and large-bore strong magnets because magnetic effects would be more remarkable in the high SMF. Additionally, fabricating large-size samples is limited in a small bore magnet. Another reason is that a high-cost magnet limits a wide application of the SMF. Reassuringly, the rapid development of low-cost room-temperature superconducting materials is expected to open up prospects for the application of the SMF in industrial applications.

(2) Development of in-situ SMF testing devices for high temperature

Thermophysical parameters should be considered carefully since the SMF, especially a high SMF, may change the values of the thermophysical parameters of metallic materials. Hence, it is imperative to exploit an in-situ SMF device to detect the variation in solidification parameters, such as thermoelectric current and melt flow velocity. Meanwhile, the in-situ measurement of the SMF is conducive to revealing the physical nature of solidification phenomena in the SMF. Although a few scientific apparatuses have been developed, such as thermal analysis apparatus and tensiometer, more standard and commercial instruments should be developed to be adaptable to the conditions of high temperatures in the SMF.

(3) Fundamentals of magnetic effects

Materials processing in the SMF is a new interdisciplinary field. Although many new phenomena have been discovered over the past decades, a lot of fundamental scientific questions in the SMF including nucleation, growth, interfacial phenomena, diffusion, etc., are still to be clarified. Furthermore, more processing methods in combination with the SMF are expected to bring forward the optimization of microstructures and mechanical properties of metallic materials. Hopefully, the SMF will become a general and powerful tool to control solidification processing in practical application in materialists' and metallurgists' efforts in the near future.

Author Contributions: Conceptualization, C.L.; writing—original draft preparation, Y.H.; writing—review and editing, Z.G. and C.L. All authors have read and agreed to the published version of the manuscript.

Funding: This work was supported financially by Natural Science Foundation of China (52127807), Natural Science Foundation of Inner Mongolia Autonomous Region (2020BS05018) and Science and Technology Plan of Inner Mongolia Autonomous Region (2022YFHH0098).

Institutional Review Board Statement: Not applicable.

Informed Consent Statement: Not applicable.

Data Availability Statement: Not applicable.

Conflicts of Interest: The authors declare no conflict of interests.

References

1. Kurz, W.; Fisher, D.J. *Fundamentals of Solidification*, 3rd ed.; Trans Tech Pubications: Aedermannsdorf, Switzerland, 1992; pp. 1–15.
2. Flemings, M.C. Solidification processing. *Metall. Mater. Trans. B* **1974**, *5*, 2121–2134. [CrossRef]
3. Asta, M.; Beckermann, C.; Karma, A.; Kurz, W.; Napolitano, R.; Plapp, M.; Purdy, G.; Rappaz, M.; Trivedi, R. Solidification microstructures and solid-state parallels: Recent developments, future directions. *Acta Mater.* **2009**, *57*, 941–971. [CrossRef]
4. Chen, G.; Zheng, G.; Qi, Z.; Zhang, J.; Li, P.; Cheng, J.; Zhang, Z. Research progress on controlled solidification and its applications. *Acta Metall. Sin.* **2018**, *54*, 669–681.
5. Suthar, J.; Persis, J.; Gupta, R. Critical parameters influencing the quality of metal castings: A systematic literature review. *Int. J. Qual. Reliab. Manage.* 2021, *ahead-of-print*. [CrossRef]
6. Eskin, D.G.; Mi, J. *Solidification Processing of Metallic Alloys under External Fields*, 1st ed.; Springer: Cham, Switzerland, 2018; pp. 75–275.
7. Hu, S.; Chen, L.; Zhou, Q.; Wang, J. Research progress in effects of physical fields on solidified structure of metals. *Spec. Cast. Nonferr. Alloy.* **2018**, *38*, 717–720.
8. Asai, S. Recent development and prospect of electromagnetic processing of materials. *Sci. Technol. Adv. Mat.* **2000**, *1*, 191–200. [CrossRef]
9. Cho, S.; Thomas, B.G. Electromagnetic forces in continuous casting of steel slabs. *Metals* **2019**, *9*, 471. [CrossRef]
10. Li, X.; Ren, Z. Thermoelectric magnetic effect and its effect on the solidification structure under static magnetic fields. *Mater. China* **2014**, *33*, 349–354.
11. Magomedov, M.N. On the magnetic-field-induced changes in the parameters of phase transitions. *Tech. Phys. Lett.* **2002**, *28*, 116–118. [CrossRef]
12. Ren, Z.; Lei, Z.; Li, C.; Xuan, W.; Zhong, Y.; Li, X. New study and development on electromagnetic field technology in metallurgical processes. *Acta Metall. Sin.* **2020**, *56*, 583–600.
13. Zhao, Z.; Chai, Y.; Zheng, S.; Wang, L.; Xiao, Y. Electromagnetic field assisted metallic materials processing: A review. *Steel Res. Int.* **2017**, *88*, 1600273. [CrossRef]
14. Liu, T.; Wang, Q.; Liu, F.; Li, G.; He, J. Nucleation behavior of bulk Ni–Cu alloy and pure Sb in high magnetic fields. *J. Cryst. Growth* **2011**, *321*, 167–170. [CrossRef]
15. Koyama, K.; Mitsui, Y.; Choi, E.S.; Ikehara, Y.; Palm, E.C.; Watanabe, K. Change of the equilibrium state of ferromagnetic MnBi by high magnetic fields. *J. Alloy. Compd.* **2011**, *509*, L78–L80. [CrossRef]
16. Li, C.; Cao, Y.; Lippmann, S.; Ren, Z.; Rettenmayr, M. Reduced wettability of solids by a liquid Ga–in–Sn alloy in a steady magnetic field. *J. Phys. Chem. C* **2018**, *122*, 27451–27455. [CrossRef]
17. He, S.; Zhan, T.; Li, C.; Xuan, W.; Wang, J.; Ren, Z. Enhanced dendrite coarsening and microsegregation in Al-Cu alloy under a steady magnetic field. *Mater. Trans.* **2019**, *60*, 1921–1927. [CrossRef]
18. Li, X.; Gagnoud, A.; Fautrelle, Y.; Ren, Z.; Moreau, R.; Zhang, Y.; Esling, C. Dendrite fragmentation and columnar-to-equiaxed transition during directional solidification at lower growth speed under a strong magnetic field. *Acta Mater.* **2012**, *60*, 3321–3332. [CrossRef]
19. Li, X.; Gagnoud, A.; Ren, Z.; Fautrelle, Y.; Debray, F. Effect of strong magnetic field on solid solubility and microsegregation during directional solidification of Al-Cu alloy. *J. Mater. Res.* **2013**, *28*, 2810–2818. [CrossRef]
20. Zheng, T.; Zhou, B.; Wang, J.; Shuai, S.; Zhong, Y.; Ren, W.; Ren, Z.; Debray, F.; Beaugnon, E. Compression properties enhancement of Al-Cu alloy solidified under a 29 T high static magnetic field. *Mater. Sci. Eng. A* **2018**, *733*, 170–178. [CrossRef]
21. Vives, C.; Perry, C. Effects of magnetically damped convection during the controlled solidification of metals and alloys. *Int. J. Heat Mass Transf.* **1987**, *30*, 479–496. [CrossRef]
22. Shercliff, J.A. Thermoelectric magnetohydrodynamics. *J. Fluid Mech.* **1979**, *91*, 231–251. [CrossRef]
23. Khine, Y.Y.; Walker, J.S. Thermoelectric magnetohydrodynamic effects during bridgman semiconductor crystal growth with a uniform axial magnetic field. *J. Cryst. Growth* **1999**, *183*, 150–158. [CrossRef]
24. Li, X.; Gagnoud, A.; Ren, Z.; Fautrelle, Y.; Moreau, R. Investigation of thermoelectric magnetic convection and its effect on solidification structure during directional solidification under a low axial magnetic field. *Acta Mater.* **2009**, *57*, 2180–2197. [CrossRef]
25. Asai, S. *Electromagnetic Processing of Materials*, 1st ed.; Springer: Dordrecht, The Netherlands, 2012; pp. 113–150.
26. Ren, Z.; Wang, J.; Zhao, R. Orientation and alignment during materials processing under high magnetic fields. *Chin. Phys. B* **2019**, *28*, 048301. [CrossRef]
27. Zhou, G. Nucleation thermodynamics of oxide during metal oxidation. *Appl. Phys. Lett.* **2009**, *94*, 201905. [CrossRef]
28. Sun, Z.H.I.; Guo, X.; Guo, M.; Li, C.; Vleugels, J.; Ren, Z.; Van der Biest, O.; Blanpain, B. Strong magnetic field effect on surface tension associated with an interfacial magnetic pressure. *J. Phys. Chem. C* **2012**, *116*, 17676–17681. [CrossRef]
29. Guo, R.; Li, C.; He, S.; Wang, J.; Xuan, W.; Li, X.; Zhong, Y.; Ren, Z. Enhanced undercooling of para- and diamagnetic metal melts in steady magnetic field. *Jpn. J. Appl. Phys.* **2018**, *57*, 80301. [CrossRef]
30. Guo, R.; Li, C.; He, S.; Wang, J.; Xuan, W.; Li, X.; Zhong, Y.; Ren, Z. Effect of steady magnetic field on undercooling of Al-Cu alloy melts. *Europhys. Lett.* **2019**, *126*, 46001. [CrossRef]
31. Guo, R.; Shuai, S.; Zhao, R.; Li, C.; Li, X.; Zhong, Y.; Wang, J.; Ren, Z. Enhanced degradation in grain refinement of inoculated 2024 Al alloy in steady magnetic field. *Metall. Mater. Trans. A* **2020**, *51*, 4584–4591. [CrossRef]

32. Wang, J.; He, Y.; Li, J.; Kou, H.; Beaugnon, E. Reexaminations of the effects of magnetic field on the nucleation of undercooled Cu melt. *Jpn. J. Appl. Phys.* **2016**, *55*, 105601. [CrossRef]
33. Wang, J.; He, Y.; Li, J.; Kou, H.; Beaugnon, E. Strong magnetic field effect on the nucleation of a highly undercooled Co-Sn melt. *Sci. Rep.* **2017**, *7*, 4958. [CrossRef]
34. Iino, M.; Fujimura, Y. Surface tension of heavy water under high magnetic fields. *Appl. Phys. Lett.* **2009**, *94*, 1641. [CrossRef]
35. Li, C.; Chen, L.; Ren, Z. Surface tensions of non-polar liquids in high magnetic fields. *J. Mol. Liq.* **2013**, *181*, 51–54. [CrossRef]
36. Böyük, U.; Engin, S.; Maraşlı, N. Novel experimental technique to observe equilibrated grain boundary groove shapes in opaque alloys. *J. Alloy. Compd.* **2009**, *476*, 213–219. [CrossRef]
37. Glicksman, M.E.; Vold, C.L. Determination of absolute solid-liquid interfacial free energies in metals. *Acta Metall.* **1969**, *17*, 1–11. [CrossRef]
38. Gündüz, M.; Hunt, J.D. The measurement of solid-liquid surface energies in the Al-Cu, Al-Si and Pb-Sn systems. *Acta Metall.* **1985**, *33*, 1651–1672. [CrossRef]
39. Maeda, K.; Niitsu, A.; Morito, H.; Shiga, K.; Fujiwara, K. In situ observation of grain boundary groove at the crystal/melt interface in Cu. *Scr. Mater.* **2018**, *146*, 169–172. [CrossRef]
40. Maraşli, N.; Hunt, J.D. Solid-liquid surface energies in the Al-$CuAl_2$, Al-$NiAl_3$ and Al-Ti systems. *Acta Mater.* **1996**, *44*, 1085–1096. [CrossRef]
41. Liu, T.; Xiao, Y.; Lu, Z.; Hirota, N.; Li, G.; Yuan, S.; Wang, Q. Wetting Behaviors of molten melt drops on polycrystalline Al_2O_3 substrates in high magnetic fields. *J. Mater. Sci. Technol.* **2020**, *41*, 187–190. [CrossRef]
42. Huang, C.; Shuai, S.; Wang, P.; Liu, X.; Wang, J.; Ren, Z. The effect of static magnetic field on solid-liquid interfacial free energy of Al-Cu alloy system. *Scr. Mater.* **2020**, *187*, 232–236. [CrossRef]
43. Gao, J.; Han, M.; Kao, A.; Pericleous, K.; Alexandrov, D.V.; Galenko, P.K. Dendritic growth velocities in an undercooled melt of pure nickel under static magnetic fields: A test of theory with convection. *Acta Mater.* **2016**, *103*, 184–191. [CrossRef]
44. Gao, J.; Kao, A.; Bojarevics, V.; Pericleous, K.; Galenko, P.K.; Alexandrov, D.V. Modeling of convection, temperature distribution and dendritic growth in glass-fluxed nickel melts. *J. Cryst. Growth.* **2017**, *471*, 66–72. [CrossRef]
45. Basaran, M. Dendrite coarsening and microsegregation in Al-Cu alloys. *Metall. Trans. A* **1981**, *12*, 1235–1243. [CrossRef]
46. Combeau, H.; Drezet, J.M.; Mo, A.; Rappaz, M. Modeling of microsegregation in macrosegregation computations. *Metall. Mater. Trans. A* **1996**, *27*, 2314–2327. [CrossRef]
47. Kirkwood, D.H. Microsegregation. *Mater. Sci. Eng.* **1984**, *65*, 101–109. [CrossRef]
48. Kraft, T.; Chang, Y.A. Discussion of "effect of dendrite arm coarsening on microsegregation". *Metall. Mater. Trans. A* **1998**, *29*, 2447–2449. [CrossRef]
49. Lacaze, J.; Lesoult, G. Modelling the development of microsegregation during solidification of an Al-Cu-Mg-Si alloy. *ISIJ Int.* **1995**, *35*, 658–664. [CrossRef]
50. Mortensen, A. On the influence of coarsening on microsegregation. *Metall. Trans. A* **1989**, *20*, 247–253. [CrossRef]
51. Terzi, S.; Salvo, L.; Suery, M.; Dahle, A.K.; Boller, E. Coarsening mechanisms in a dendritic Al–10% Cu alloy. *Acta Mater.* **2010**, *58*, 20–30. [CrossRef]
52. Voller, V.R. A model of microsegregation during binary alloy solidification. *Int. J. Heat Mass Tran.* **2000**, *43*, 2047–2052. [CrossRef]
53. Li, X.; Fautrelle, Y.; Ren, Z. Influence of thermoelectric effects on the solid–liquid interface shape and cellular morphology in the mushy zone during the directional solidification of Al-Cu alloys under a magnetic field. *Acta Mater.* **2007**, *55*, 3803–3813. [CrossRef]
54. Moreau, R.; Laskar, O.; Tanaka, M.; Camel, D. Thermoelectric magnetohydrodynamic effects on solidification of metallic alloys in the dendritic regime. *Mater. Sci. Eng. A* **1993**, *173*, 93–100. [CrossRef]
55. Tewari, S.N.; Shah, R. Macrosegregation during dendritic arrayed growth of hypoeutectic Pb-Sn alloys: Influence of primary arm spacing and mushy zone length. *Metall. Mater. Trans. A* **1996**, *27*, 1353–1362. [CrossRef]
56. Zhong, H.; Li, C.; Ren, Z.; Rettenmayr, M.; Zhong, Y.; Yu, J.; Wang, J. Effect of interdendritic thermoelectric magnetic convection on evolution of tertiary dendrite during directional solidification. *J. Cryst. Growth* **2016**, *439*, 66–73. [CrossRef]
57. Bhadeshia, H.K.D.H. Steels for bearings. *Prog. Mater. Sci.* **2012**, *57*, 268–435. [CrossRef]
58. Dong, Z.; Jiang, B.; Mei, Z.; Zhang, C.; Zhou, L.; Liu, Y. Effect of carbide distribution on the grain refinement in the steel for large-size bearing ring. *Steel Res. Int.* **2016**, *87*, 745–751. [CrossRef]
59. Grong, Ø.; Kolbeinsen, L.; van der Eijk, C.; Tranell, G. Microstructure control of steels through dispersoid metallurgy using novel grain refining alloys. *ISIJ Int.* **2006**, *46*, 824–831. [CrossRef]
60. Qiu, H.; Wang, L.; Hanamura, T.; Torizuka, S. Physical interpretation of grain refinement-induced variation in fracture mode in ferritic steel. *ISIJ Int.* **2013**, *53*, 382–384. [CrossRef]
61. Jin, T.N.; Nie, Z.R.; Guo-Fu, X.U. Effects of cooling rate on solidification behavior of dilute Al-Sc and Al-Sc-Zr solid solution. *T. Nonferr. Metal. Soc.* **2004**, *14*, 58–62.
62. Kivi, M.; Holappa, L.; Iung, T. Addition of dispersoid titanium oxide inclusions in steel and their influence on grain refinement. *Metall. Mater. Trans. B* **2010**, *41*, 1194–1204. [CrossRef]
63. Sasaki, M.; Ohsasa, K.; Kudoh, M.; Matsuura, K. Refinement of austenite grain in carbon steel by addition of titanium and boron. *ISIJ Int.* **2008**, *48*, 340–343. [CrossRef]

64. Li, X.; Fautrelle, Y.; Zaidat, K.; Gagnoud, A.; Ren, Z.; Moreau, R.; Zhang, Y.; Esling, C. Columnar-to-equiaxed transitions in Al-based alloys during directional solidification under a high magnetic field. *J. Cryst. Growth* **2010**, *312*, 267–272. [CrossRef]
65. Li, X.; Ren, Z.; Shen, Y.; Fautrelle, Y. Effect of Thermoelectric magnetic force on the array of dendrites during directional solidification of Al-Cu alloys in a high magnetic field. *Phil. Mag. Lett.* **2012**, *92*, 675–682. [CrossRef]
66. Yu, J.; Du, D.; Ren, Z.; Fautrelle, Y.; Moreau, R.; Li, X. Influence of an axial magnetic field on microstructures and alignment in directionally solidified Ni-based superalloy. *ISIJ Int.* **2017**, *57*, 337–342. [CrossRef]
67. Hou, Y.; Zhang, Z.; Xuan, W.; Wang, J.; Yu, J.; Ren, Z. Grain refinement during directionally solidifying GCr18Mo steel at low pulling speeds under an axial static magnetic field. *Acta Metall. Sin-Engl.* **2018**, *31*, 681–691. [CrossRef]
68. Hou, Y.; Ren, Z.; Zhang, Z.; Ren, X. Columnar to equiaxed transition during directionally solidifying GCr18Mo steel affected by thermoelectric magnetic force under an axial static magnetic field. *ISIJ Int.* **2019**, *59*, 60–68. [CrossRef]
69. Kobayashi, Y.; Todoroki, H.; Mizuno, K. Problems in solidification model for microsegregation analysis of Fe-Cr-Ni-Mo-Cu alloys. *ISIJ Int.* **2019**, *59*, 277–282. [CrossRef]
70. Lynch, P.C.; Grimm, T.J. Reducing Microsegregation in next-generation high-strength low-alloy cast steels. *Int. J. Metalcast.* **2019**, *13*, 783–792. [CrossRef]
71. Hou, L.; Dai, Y.; Fautrelle, Y.; Li, Z.; Ren, Z.; Esling, C.; Li, X. Evolution of microstructure and microsegregation in Ni-Mn-Ga alloys directionally solidified under axial magnetic field. *J. Alloy. Compd.* **2018**, *758*, 54–61. [CrossRef]
72. Ren, W.; Lu, L.; Yuan, G.; Xuan, W.; Zhong, Y.; Yu, J.; Ren, Z. The effect of magnetic field on precipitation phases of single-crystal Nickel-base superalloy during directional solidification. *Mater. Lett.* **2013**, *100*, 223–226. [CrossRef]
73. Song, J.Y.; Zhao, X.; Zhang, Y.D.; Esling, C.; Zuo, L. Influence of a high magnetic field on the solubility of ferrite and the amount of pearlite. *Steel Res. Int.* **2011**, *82*, 836–838. [CrossRef]
74. Zhang, T.; Ren, W.; Dong, J.; Li, X.; Ren, Z.; Cao, G.; Zhong, Y.; Deng, K.; Lei, Z.; Guo, J. Effect of high magnetic field on the primary dendrite arm spacing and segregation of directionally solidified superalloy DZ417G. *J. Alloy. Compd.* **2009**, *487*, 612–617. [CrossRef]
75. He, S.; Li, C.; Guo, R.; Xuan, W.; Wang, J.; Ren, Z. Evolution of microsegregation in directionally solidified Al-Cu alloys under steady magnetic field. *J. Alloy. Compd.* **2019**, *800*, 41–49. [CrossRef]
76. Hardin, R.A.; Beckermann, C. Effect of porosity on the stiffness of cast steel. *Metall. Mater. Trans. A* **2007**, *38*, 2992–3006. [CrossRef]
77. Dong, Q.; Zhang, J.; Wang, B.; Zhao, X. Shrinkage porosity and its alleviation by heavy reduction in continuously cast strand. *J. Mater. Process. Tech.* **2016**, *238*, 81–88. [CrossRef]
78. Li, J.; Wang, B.; Ma, Y.; Cui, J. Effect of complex electromagnetic stirring on inner quality of high carbon steel bloom. *Mater. Sci. Eng. A* **2006**, *425*, 201–204. [CrossRef]
79. Li, Y.; Li, L.; Zhang, J. Study and application of a simplified soft reduction amount model for improved internal quality of continuous casting bloom. *Steel Res. Int.* **2017**, *88*, 1700176. [CrossRef]
80. Zeng, J.; Chen, W.; Zhang, S.; Li, Y.; Wang, Q. Development and application of final permanent magnet stirring during continuous casting of high carbon rectangular billet. *ISIJ Int.* **2015**, *55*, 2142–2149. [CrossRef]
81. Hou, Y.; Shuai, S.; Dong, Y.; Xuan, W.; Wang, J.; Zhang, Z.; Ren, X.; Ren, Z. Effect of thermoelectric magnetic convection on shrinkage porosity at the final stage of solidification of GCr18Mo steel under axial static magnetic field. *Metall. Mater. Trans. B* **2019**, *50*, 881–889. [CrossRef]
82. Mikelson, A.E.; Karklin, Y.K. Control of crystallization processes by means of magnetic fields. *J. Cryst. Growth* **1981**, *52*, 524–529. [CrossRef]
83. Molodov, D.A.; Konijnenberg, P.J. Grain boundary and grain structure control through application of a high magnetic field. *Scr. Mater.* **2006**, *54*, 977–981. [CrossRef]
84. Zheng, T.; Zhong, Y.; Lei, Z.; Ren, W.; Ren, Z.; Wang, H.; Wang, Q.; Debray, F.; Beaugnon, E.; Fautrelle, Y. Effects of high static magnetic field on crystal orientation and magnetic property of Bi-5Wt.% Zn alloys. *Mater. Lett.* **2015**, *140*, 68–70. [CrossRef]
85. Wang, H.; Ren, Z.; Deng, K.; Xu, K. Effects of a static magnetic field on solidification structure of MnBi Phase in semi-solidified Bi-Mn alloy. *Acta Metall. Sin.* **2002**, *38*, 41–46.
86. Han, Y.; Ban, C.; Guo, S.; Liu, X.; Ba, Q.; Cui, J. Alignment behavior of primary Al_3Fe Phase in Al-Fe alloy under a high magnetic field. *Mater. Lett.* **2007**, *61*, 983–986. [CrossRef]
87. Liu, Y.; Wang, Q.; Liu, T.; Gao, P.; Yuan, Y.; He, J. Effects of high magnetic fields on the crystal orientation and magnetostriction of a $TbFe_2$ based alloy during treatment in the semi-solid state. *J. Alloy. Compd.* **2014**, *590*, 110–115. [CrossRef]
88. Cheng, L.; Zhang, N.; Yang, P.; Mao, W.M. Retaining {100} texture from initial columnar grains in electrical steels. *Scr. Mater.* **2012**, *67*, 899–902. [CrossRef]
89. Sha, Y.H.; Sun, C.; Zhang, F.; Patel, D.; Chen, X.; Kalidindi, S.R.; Zuo, L. Strong cube recrystallization texture in silicon steel by twin-roll casting process. *Acta Mater.* **2014**, *76*, 106–117. [CrossRef]
90. Liu, C.; Zhong, Y.; Shen, Z.; Zheng, T.; Dong, L.; Ren, W.; Lei, Z.; Ren, Z. Effect of an axial high static magnetic field on the crystal orientation and magnetic property of Fe-4.5 Wt% Si alloy during bulk solidification. *Mater. Lett.* **2019**, *247*, 189–192. [CrossRef]
91. Liu, C.; Zhong, Y.; Shen, Z.; Dong, L.; Zheng, T.; Ren, W.; Lei, Z.; Ren, Z. Effect of a transverse weak magnetic field on the texture evolution and magnetic property of Fe-1.0 Wt.% Si alloy during bulk solidification. *Mater. Res. Express* **2019**, *6*, 066105. [CrossRef]
92. Liu, C.; Zhong, Y.; Shen, Z.; Dong, L.; Zheng, T.; Ren, W.; Lei, Z.; Ren, Z. Magnetic field–dependent microstructure evolution and magnetic property of Fe–6.5 Si–0.05 B alloy during solidification. *J. Mater. Res.* **2019**, *34*, 4076–4084. [CrossRef]

93. DebRoy, T.; Wei, H.L.; Zuback, J.S.; Mukherjee, T.; Elmer, J.W.; Milewski, J.O.; Beese, A.M.; Wilson-Heid, A.; De, A.; Zhang, W. Additive manufacturing of metallic components-process, structure and properties. *Prog. Mater. Sci.* **2018**, *92*, 112–224. [CrossRef]
94. Frazier, W.E. Metal additive manufacturing: A review. *J. Mater. Eng. Perform.* **2014**, *23*, 1917–1928. [CrossRef]
95. Murphy, S.V.; Atala, A. 3D bioprinting of tissues and organs. *Nat. Biotechnol.* **2014**, *32*, 773–785. [CrossRef] [PubMed]
96. Ngo, T.D.; Kashani, A.; Imbalzano, G.; Nguyen, K.T.Q.; Hui, D. Additive manufacturing (3D printing): A review of materials, methods, applications and challenges. *Compos. Part B-Eng.* **2018**, *143*, 172–196. [CrossRef]
97. Al-Bermani, S.S.; Blackmore, M.L.; Zhang, W.; Todd, I. The origin of microstructural diversity, texture, and mechanical properties in electron beam melted Ti-6Al-4V. *Metall. Mater. Trans. A* **2010**, *41*, 3422–3434. [CrossRef]
98. Li, X.P.; Ji, G.; Chen, Z.; Addad, A.; Wu, Y.; Wang, H.W.; Vleugels, J.; Van Humbeeck, J.; Kruth, J.P. Selective laser melting of nano-TiB_2 decorated AlSi10Mg alloy with high fracture strength and ductility. *Acta Mater.* **2017**, *129*, 183–193. [CrossRef]
99. Yu, J.; Rombouts, M.; Maes, G.; Motmans, F. Material properties of Ti6Al4V parts produced by laser metal deposition. *Phys. Procedia* **2012**, *39*, 416–424. [CrossRef]
100. Zhao, R.; Chen, C.; Shuai, S.; Hu, T.; Fautrelle, Y.; Liao, H.; Lu, J.; Wang, J.; Ren, Z. Enhanced mechanical properties of Ti6Al4V alloy fabricated by laser additive manufacturing under static magnetic field. *Mater. Res. Lett.* **2022**, *10*, 530–538. [CrossRef]
101. Liu, X.; Yu, J.; Shuai, S.; Xuan, W.; Wang, J.; Ren, Z. Cell-to-dendrite transition induced by a static transverse magnetic field during lasering remelting of the Nickel-based superalloy. *Metall. Mater. Trans. B* **2018**, *49*, 3211–3219. [CrossRef]
102. Nie, J.; Chen, C.; Shuai, S.; Liu, X.; Zhao, R.; Wang, J.; Liao, H.; Ren, Z. Effect of static magnetic field on the evolution of residual stress and microstructure of laser remelted Inconel 718 superalloy. *J. Therm. Spray Techn.* **2020**, *29*, 1410–1423. [CrossRef]
103. Zhu, W.; Yu, S.; Chen, C.; Shi, L.; Xu, S.; Shuai, S.; Hu, T.; Liao, H.; Wang, J.; Ren, Z. Effects of static magnetic field on the microstructure of selective laser melted Inconel 625 superalloy: Numerical and experiment investigations. *Metals* **2021**, *11*, 1846. [CrossRef]
104. Kang, N.; Yuan, H.; Coddet, P.; Ren, Z.; Bernage, C.; Liao, H.; Coddet, C. On the texture, phase and tensile properties of commercially pure Ti produced via selective laser melting assisted by static magnetic field. *Mater. Sci. Eng. C* **2017**, *70*, 405–407. [CrossRef] [PubMed]
105. Cai, B.; Wang, J.; Kao, A.; Pericleous, K.; Phillion, A.B.; Atwood, R.C.; Lee, P.D. 4D synchrotron X-ray tomographic quantification of the transition from cellular to dendrite growth during directional solidification. *Acta Mater.* **2016**, *117*, 160–169. [CrossRef]
106. Daudin, R.; Terzi, S.; Lhuissier, P.; Tamayo, J.; Scheel, M.; Babu, N.H.; Eskin, D.G.; Salvo, L. Particle-induced morphological modification of Al alloy equiaxed dendrites revealed by sub-second in situ microtomography. *Acta Mater.* **2017**, *125*, 303–310. [CrossRef]
107. Song, Z.; Magdysyuk, O.V.; Sparks, T.; Chiu, Y.; Cai, B. Revealing Growth Mechanisms of Faceted Al_2Cu Intermetallic Compounds Via High-Speed Synchrotron X-Ray Tomography. *Acta Mater.* **2022**, *231*, 117903. [CrossRef]
108. Fautrelle, Y.; Wang, J.; Salloum-Abou-Jaoude, G.; Abou-Khalil, L.; Reinhart, G.; Li, X.; Ren, Z.M.; Nguyen-Thi, H. Thermo-electric-magnetic hydrodynamics in solidification: In situ observations and theory. *JOM* **2018**, *70*, 764–771. [CrossRef]
109. Wang, J.; Fautrelle, Y.; Ren, Z.M.; Li, X.; Nguyen-Thi, H.; Mangelinck-Noel, N.; Salloum, A.; Zhong, Y.B.; Kaldre, I.; Bojarevics, A. Thermoelectric magnetic force acting on the solid during directional solidification under a static magnetic field. *Appl. Phys. Lett.* **2012**, *101*, 1331–1333.
110. Wang, J.; Fautrelle, Y.; Ren, Z.M.; Nguyen-Thi, H.; Salloum Abou Jaoude, G.; Reinhart, G.; Mangelinck-Noël, N.; Li, X.; Kaldre, I. Thermoelectric magnetic flows in melt during directional solidification. *Appl. Phys. Lett.* **2014**, *104*, 121916.
111. Wang, J.; Fautrelle, Y.; Nguyen-Thi, H.; Reinhart, G.; Liao, H.; Li, X.; Zhong, Y.; Ren, Z. Thermoelectric magnetohydrodynamic flows and their induced change of solid–liquid interface shape in static magnetic field-assisted directional solidification. *Metallur. Mater. Trans. A* **2016**, *47*, 1169–1179. [CrossRef]
112. Yasuda, H.; Inoue, K.; Minami, Y.; Nagira, T.; Yoshiya, M.; Uesugi, K.; Umetani, K. Direct observation of thermoelectric magnetic convection in unidirectionally solidified Al-Cu alloys. *J. Iron Steel Res. Int.* **2012**, *19*, 34–39.
113. Wang, J.; Lin, X.; Fautrelle, Y.; Nguyen-Thi, H.; Ren, Z. Motion of solid grains during magnetic field-assisted directional solidification. *Metall. Mater. Trans. B* **2018**, *49*, 861–865. [CrossRef]
114. Abou-Khalil, L.; Wang, J.; Salloum-Abou-Jaoude, G.; Garrido, M.; Li, X.; Ren, Z.; Reinhart, G.; Nguyen-Thi, H.; Fautrelle, Y. Investigation of thermo-electro-magnetic force on equiaxed grain motion during upward directional solidification. *Int. J. Therm. Sci.* **2019**, *145*, 106047. [CrossRef]
115. Cai, B.; Kao, A.; Boller, E.; Magdysyuk, O.V.; Atwood, R.C.; Vo, N.T.; Pericleous, K.; Lee, P.D. Revealing the Mechanisms by Which Magneto-Hydrodynamics Disrupts Solidification Microstructures. *Acta Mater.* **2020**, *196*, 200–209. [CrossRef]
116. Li, X.; Fautrelle, Y.; Gagnoud, A.; Moreau, R.; Du, D.; Ren, Z.; Lu, X. EBSD study on the effect of a strong axial magnetic field on the microstructure and crystallography of Al-Ni alloys during solidification. *Metall. Mater. Trans. A* **2016**, *47*, 1180–1197. [CrossRef]
117. Shuai, S.; Lin, X.; Dong, Y.; Hou, L.; Liao, H.; Wang, J.; Ren, Z. Three dimensional dendritic morphology and orientation transition induced by high static magnetic field in directionally solidified Al-10 Wt.%Zn alloy. *J. Mater. Sci. Technol.* **2019**, *35*, 1587–1592. [CrossRef]
118. Cao, J.; Shuai, S.; Huang, C.; Hu, T.; Chen, C.; Wang, J.; Ren, Z. 4D synchrotron X-Ray tomographic study of the influence of transverse magnetic field on iron intermetallic compounds precipitation behavior during solidification of Al-Si-Fe alloy. *Intermetallics* **2022**, *143*, 107471. [CrossRef]